

This document is the unedited Author's version of a Submitted Work that was subsequently accepted for publication in ACS Applied Energy Materials, copyright © American Chemical Society after peer review. To access the final edited and published work see <https://pubs.acs.org/doi/10.1021/acsaem.1c00675>

Access to this work was provided by the University of Maryland, Baltimore County (UMBC) ScholarWorks@UMBC digital repository on the Maryland Shared Open Access (MD-SOAR) platform.

**Please provide feedback**

Please support the ScholarWorks@UMBC repository by emailing [scholarworks-group@umbc.edu](mailto:scholarworks-group@umbc.edu) and telling us what having access to this work means to you and why it's important to you. Thank you.

# Rechargeable Zinc – Electrolytic manganese dioxide (EMD) battery with a flexible chitosan alkaline electrolyte.

*Aswani Poosapati,<sup>a</sup> Sudharshan Vadhana,<sup>a</sup> Karla Negrete,<sup>a</sup> Yucheng Lan,<sup>b</sup> John Hutchison,<sup>a</sup> Mark Zupan,<sup>a</sup> and Deepa Madan<sup>a,\*</sup>*

<sup>a</sup> University of Maryland Baltimore County, Department of Mechanical Engineering, Engineering building, 1000 Hilltop circle, MD 21250

<sup>b</sup> Morgan state university, Department of Physics, 1700 E Cold Spring Ln, MD 21251.

\* **Correspondence** to Dr. Deepa Madan (deemadan@umbc.edu)

## Abstract

A high performing flexible chitosan-based gel electrolyte with poly-vinyl alcohol (PVA) additive was prepared and swelled in varying concentrations of potassium hydroxide (KOH) solutions. A highest ionic conductivity of 457 mS/cm was recorded for the sample with a 2.1 swelling ratio, obtained by soaking in 5M KOH solution for 45 minutes. Stability tests results demonstrated the prepared electrolyte to be strong and ductile along with stability under 50°C and 2 V. Zn-EMD batteries were constructed with the prepared electrolyte using an optimized assembly technique employed to achieve good interfacial contact between the layers. Continuous charge-discharge tests were performed on the batteries at a current density of 0.1 A/g in specific limited and extended potential regions (low: 0.4-1.2 V and high: 0.4-1.6 V) to explore their performance and

reversibility. Results indicated that the batteries cycled in the low region had higher capacity retention due to lower  $\delta$ -MnO<sub>2</sub> formations when compared to high region cycling. To fully understand its performance capability, the battery was further tested extensively. Results indicated a good rate and initial bending performance of the battery with a maximum specific capacity of 310 mAh/g at 0.1 A/g. Additionally, the battery tested at 0.5 A/g showed an average specific capacity of 175 mAh/g over 300 cycles with 96.5% coulombic efficiency. Attaining energy densities between 150.4 – 252.4 Wh/kg (w.r.t active cathode mass) is possible for these batteries, thus encouraging their use in varied applications. Utilizing chitosan gel electrolyte and limited voltage window testing, the prepared Zn-EMD alkaline batteries are among the first reported polymer-based alkaline electrolyte Zn rechargeable batteries with no cathode additives.

## **Keywords**

Chitosan based electrolyte, Poly (vinyl alcohol), potassium hydroxide, activated carbon cloth, rechargeable, Zinc-Electrolytic manganese dioxide alkaline battery.

## **Introduction**

Although there exists reliable, efficient, and scalable lithium based rechargeable batteries today, the need for much safer and cost-effective energy storage devices have prominently driven research towards alternative chemistries for decades now<sup>1-6</sup>. Recently, huge attention is directed towards multivalent cations intercalation chemistries such as Zn<sup>2+</sup>, Mg<sup>2+</sup>, Ca<sup>2+</sup> and Al<sup>3+</sup><sup>6-9</sup>, due to the advantages of their multiple electron transfers. Amongst the latter, Zn<sup>2+</sup> based batteries have

gained more popularity due to the abundance of metallic zinc: its low toxicity, intrinsic safety, reliable electrochemical performance, smaller ionic radius ( $0.74 \text{ \AA}$ ), high volumetric capacity ( $5850 \text{ mAh/cm}^3$ ), easy disposal, and also its ability to remain stable in ambient air <sup>5, 6</sup>. To boost their application in flexible energy storage systems such as wearables or flexible electronics, incorporation of flexible electrolytes supporting zinc based chemistries plays a crucial role. Amidst various electrolytes, polymer-based have attracted a lot of attention in research due to advantages such as non-toxicity, no leakage issues, elimination of the need for separators, mechanical resistance to structural changes, and lightweight in addition to the ease involved in achievability of desired flexibility by blend of different additives <sup>5,6,10-23</sup>.

Decent performances of polymer electrolytes such as PEO<sup>10,11</sup>, PEG<sup>12</sup>, PVDF<sup>13</sup>, PVA<sup>12,14-17</sup>, PC<sup>13,18</sup>, EC<sup>13,18</sup>, PAA<sup>14,19</sup>, PEGDE<sup>11</sup>, Gelatin<sup>19-21</sup> etc. were already reported, but most preparation processes were complex and energy intensive <sup>11-16,18-20</sup>. Additionally, high interfacial resistances due to poor solubility of salts and poor adhesion between layers, limited flexibility, and lower performance efficiencies at lower temperatures due to their crystalline nature were observed <sup>11,13</sup>. Another interesting observation made was that most polymers researched upon and tested in varied battery chemistries were mostly synthetic, which are widely known for their very slow degradation rate leading to unintended environmental waste footprint <sup>22, 23</sup>. Previously, we have reported decently performing biodegradable alkaline electrolytes using nanofiber cellulose hydrogel and chitosan with additives <sup>17, 21, 24</sup>. This study devises a further enhanced chitosan-based polymer gel electrolyte with various additives using our previously optimized gel-polymer preparation

technique, and also includes its incorporation in Zn-EMD systems to test its compatibility and performance.

Chitosan with PVA {CP} was chosen as the base polymer here among the previously prepared biodegradable polymers due to its good solvent retention capacity, flexibility, high-temperature stability, eco-friendliness, ease of preparation, amorphicity, self-gelatinous nature. These attributes facilitate enhanced film preparation and high ionic conductivity ( $\sim 6.95$  mS/cm)<sup>24,25</sup>. Ion incorporation into the CP sample was performed by allowing it to swell in varying molar concentrations of the alkaline solution for varied times. Potassium hydroxide (KOH) was specifically chosen among the various commonly used (NaOH, KOH, LiOH, etc.) alkaline mediums in rechargeable zinc batteries due to the higher ionic molar conductivity of  $K^+$  (73.5 S.cm<sup>2</sup>/equiv.), its high solubility, fast-electrochemical kinetics, and proven ability to increase ionic conductivities<sup>6,11,14,15,17,19 24,26</sup>. A highest ionic conductivity of 457.19 mS/cm was obtained for CP films with 156-218  $\mu$ m thickness soaked in 5M KOH solution for 45 min. This best performing chitosan polymer electrolyte was chosen for testing in an in-house prepared and assembled Zn-based battery.

Zn-MnO<sub>2</sub> was carefully selected among various zinc-based chemistries for testing due to its safety, abundant availability, non-flammability, reasonable output voltage (0.8-1.5 V), mercury-free nature, comparable areal capacities (1-4 mAh/cm<sup>2</sup>), high capacity for utilization (Zn-820 mAh/g, MnO<sub>2</sub>-617 mAh/g), and high energy densities (>500 Wh/kg)<sup>27-30</sup>. Amongst various forms of MnO<sub>2</sub>, EMD (also termed  $\gamma$ -MnO<sub>2</sub>): a more chemically and electrochemically active

polymorph<sup>29</sup> was picked for battery construction as it is known to show better results within alkaline cells, due to its high manganese content and purity<sup>28,30-32</sup>. Despite EMDs favourable attributes, i.e. low production cost, low toxicity, high capacity, and natural abundance, there remain challenges involving cycle life due to irreversible polymorphic changes in the chemical structure of EMD to  $\delta$ -MnO<sub>2</sub> after initial discharge<sup>27-32</sup>. However recent advancements in cell architecture and electrolyte flow achieved along with either limiting potentials, increasing charge rates and/or use of additives for this chemistry as a rechargeable system have shown to improve the cell performance<sup>27-29,32-34</sup>. Thus, EMD was chosen as the active cathode material to construct a Zn-based rechargeable battery using the devised chitosan-based gel electrolyte and employing a novel cell assembly technique to attain good contact between the solid-state gel electrolyte and electrode layers. These constructed batteries were tested and analysed in specific potential regions for their performance. Herein, we report the successful reversibility of the prepared Zn-EMD battery using the devised highly ionically conducting (457.19 mS/cm) novel electrolyte for 300 cycles with a limited voltage window of 0.4-1.2 V for charge-discharge tests. It was observed that the battery exhibited good rate performance with a highest specific capacity of 310 mAh/g and 256.2 mAh/g recorded at 0.1 and 0.5 A/g current densities respectively. Also, results indicated that energy densities within the range of 150-253 Wh/Kg (w.r.t cathode mass) were achievable for the battery cycled at 0.5 A/g.

The uniqueness of this work is the use of naturally occurring chitosan to form a highly ionically conducting (457 mS/cm) alkaline polymer electrolyte comparable to liquid electrolytes for use in

Zn-EMD batteries with no cathode additives. Though bio-degradable polymer based electrolytes were previously reported, they do not possess as high ionic conductivities and were incorporated only in super capacitors or lithium-based batteries <sup>20,35-39</sup>. Only a few polymers were used in zinc-based acidic batteries <sup>20,21</sup>. Zinc-acidic polymer electrolyte batteries uses acidic polymer electrolytes which have limited ionic conductivity (1-20mS/cm) that results in moderate capacities (~300 mAh/g) <sup>5</sup>. Zn-EMD alkaline chemistry chosen in this work is notorious for low reversibility ( due to the use of liquid electrolyte and unwanted complex irreversibile compound formation) but has added advantage of possibly achieving 617 mAh/g capacities, due to 2-electron reduction reactions if accessed (with the use of cathode additives) <sup>34</sup>. Utilizing the devised novel chitosan gel electrolyte (with high ionic conductivity 457 mS/cm) and selective voltage window for testing approach comparably good reversibility (300 cycles) (while keeping the specific capacity also high) was achieved with no additives. Previously, high reversibilities in Zn-EMD alkaline chemistry was possible only in an aqueous electrolyte medium and with cathode additives <sup>27-30,32-34</sup>.

## **Experimental**

### **Materials**

PVA (Mowiol), and KOH pellets were purchased from Sigma-Aldrich. Chitosan powder, Nitric acid, Acetone and Ethanol solutions were purchased from Fisher Scientific. Whereas, EMD (EAB 111), Ketjen black (EC-600J), W-28 (Nuosperse), Zinc foil (rolled, 99.95%, 30µm), and a flexible carbon cloth (Spectracarb 2225ACF) were purchased from Prince Int. Corp., Nouryon,

Elementis, Good fellow, and GINER ELX Inc. respectively. All were used as received without further purifications.

### **Electrolyte Preparation**

Chitosan-PVA {CP} films were prepared using a previously reported stage-wise preparation technique<sup>24</sup>. Briefly, chitosan and PVA powders were initially made solution processable. CP films were then made by drop-casting a homogeneous solution obtained by mixing chitosan and PVA solutions in 1:0.2 wt. ratio, into silicon molds and dried at 37°C overnight for 1200 min. in an oven. Dried gel electrolytes were extracted and soaked in various KOH molar concentration solutions for varied intervals (15 min– 3hrs) to obtain {X}CP films, where X=2-8M KOH. The weights of the films were measured before (W1) and after (W2) soaking at each of the time intervals of 15 min. until one hour and every 60 min. later for 3 hrs. The resultant swollen films were then tested for ionic conductivities.

### **Cathode Preparation**

A homogeneous conducting EMD cathode ink with 70:20:10 weight ratios of EMD powder, Ketjen black (conducting agent), and chitosan solution (binder) was prepared in a high energy ball milling machine (MTI corp.) at 35Hz for 30 min. A suitable amount of DI water was put in as a solvent to attain a desired, workable viscosity of the ink. A minute amount of W-28 (~2%), a dispersing agent was added to the solution, to prevent agglomerations. The final solution mixture obtained from the ball mill was used as the EMD cathode ink for battery preparation as shown in schematic figure 1(a).

## Cell Assembly

Using the best electrolyte sample ( $\{5\}$ CP), prepared EMD cathode ink, and commercially available Zinc anode foil; a complete cell was constructed. The flexible carbon cloth (CC), prior to its use as the current collector, was activated by refluxing in 3 M  $\text{HNO}_3$  solution at  $80^\circ\text{C}$  for 12 hrs. The obtained CC was then washed with acetone, ethanol, and DI water by sonication for 30 min. for each step and finally dried at  $80^\circ\text{C}$ . This acid-treated CC was then used during assembly. The homogeneous EMD cathode ink was coated on the activated CC and dried at  $110^\circ\text{C}$  for 12 hrs. The loading of the active cathode material was  $\sim 1.4 \text{ mg/cm}^2$ . The prepared stable, free-standing, flexible CP film (figure 2(a)) swelled in 5M KOH solution for 45 min., i.e.  $\{5\}$ CP electrolyte (figure 2(b), S2(a)-inset) was dipped in the CP solution to attain an even gooey coat on all its sides and then placed on the cathode. This non-conventional step of coating was employed to attain better contact of electrolyte and cathode, thereby reducing the possibilities of interfacial resistance. On top of the electrolyte, the zinc foil and another activated CC are placed one after the other. The obtained cell comprising all the five layers, as can be seen from the schematic in figure 1(a) (bottom to top – activated CC, EMD coating, coated electrolyte, Zinc foil, and activated CC), were clamped together in a swagelok cell for at least 120 min. to attain equilibrium. This equilibrated full battery was then used for testing. Additionally, a  $1.5\text{cm} \times 2\text{cm}$  cell, as in figure 1(b) was assembled using the same process as above to demonstrate flexibility.

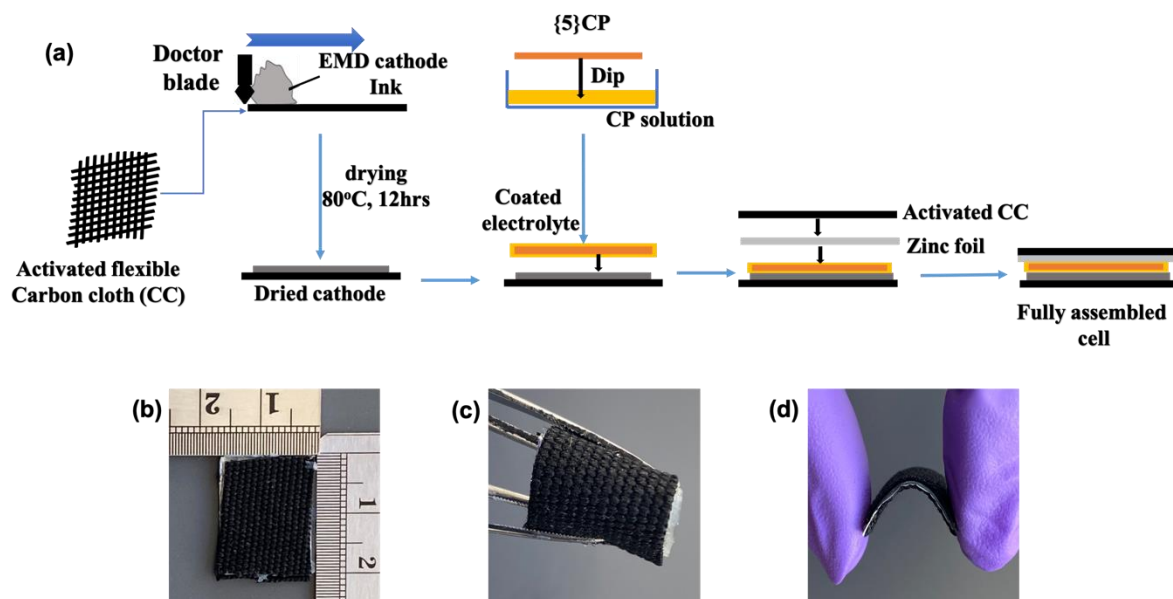


Figure 1. (a) Schematic of stages involved in Cell assembly; (b) An assembled cell with dimensions 1.5 cm x 2 cm; (c) top view and (d) side view of the assembled cell when manually bent to demonstrate flexibility.

## Characterizations

AC electrochemical impedance spectroscopy (EIS) was used to investigate ionic conductivities of samples at room temperature using a Versastat (Princeton applied research) from 1 MHz to 100 mHz at an amplitude of 10 mV. At least four samples of each of the compositions of electrolytes were made and measured to minimize the error margin. The thickness of the samples was measured using a micrometer (Mityutoyo) prior to any impedance measurements. All microscopic imaging was performed using a beam reflecting microscope (BX53M, Olympus) coupled with stream basic software for data processing of varied scans. XRD analysis was performed using a Cu-K $\alpha$  radiation source on a Rigaku mini flex operating at 15 mA and 30 kV with 0.02 degree per step rate. SEM

images were taken on a Nova NanoSEM 450 (FEI) fitted with an EDX. FTIR spectra of desired samples were measured using a Frontier Optica spectroscopy from Perkin Elmer with a resolution of  $2\text{ cm}^{-1}$ ,  $400\text{-}4000\text{ cm}^{-1}$  measuring wave number and 64 scans. TGA was conducted using a Perkin Elmer Pyris 1 thermogravimetric analyzer between  $25\text{-}325^{\circ}\text{C}$  temperature range with an increase rate of  $10^{\circ}\text{C}/\text{min}$  with He flow within the furnace. Mechanical testing was conducted on razor-cut samples through monotonic displacement control to final separation at a quasistatic strain rate of  $10^{-3}\text{ s}^{-1}$  using a custom-built loading system<sup>24</sup>. Cyclic voltammetry at  $1\text{ mV/s}$  for the low ( $0.4\text{ - }1.2\text{ V}$ ) and high ( $0.4\text{ - }1.6\text{ V}$ ) potential regions, and Linear scan voltammetry (LSV) with potential range  $0\text{ - }4\text{ V}$  at  $5\text{ mV/s}$  was performed using the earlier mentioned versastat. Charge-discharge testing of the assembled cells for their respective potential ranges and current densities was conducted using a battery cycler (MTI corp.). XPS measurements (analytical service from MSE Supplies) were obtained by employing a monochromatic Al  $K\alpha$  X-ray source with  $400\text{-micron}$  spot,  $0.05\text{ eV}$  step size, 5 scans, and  $50\text{ eV}$  pass energy.

## Results and Discussion

### Electrolyte: Swelling, Conductivity, and Stability studies

The room temperature ionic conductivities of all samples were obtained using the  $R_b$  value from AC impedance measurements of the SS/{X}CP/SS blocking electrode systems. The extracted  $R_b$  values from nyquist plots (as previous reported<sup>17,19,24</sup>), the samples thickness ( $t$ ), and the blocking electrodes area ( $A$ ) were then used to obtain the ionic conductivities of each of the samples using the equation  $\sigma_i = t/(A * R_b)$ . The base CP samples prepared had an average thickness

of 185 $\mu$ m and also were stable and flexible with no rigidity (figure 2(a)). The average ionic conductivity for the prepared batch was 7 mS/cm, three orders higher than pristine chitosan, and was similar to previously reported <sup>24</sup>. This increase was attributed to the amorphous nature of the resultant film caused due to high retention of water by PVA from solutions used during the solvent processing stage even after drying <sup>13,17,24,26,35</sup>. The concatenated optical micrograph of the translucent CP sample obtained through extended focal length image collection process shows the smooth and homogeneous surface of the prepared CP film when compared to pure chitosan (figure S1). It also shows the presence of chitosan crystals, PVA chains, and solutions trapped between them; thereby confirming the amorphous nature of the fabricated CP film. Furthermore amorphicity was validated through XRD studies and is explained in detail later.

In efforts to further improve the performance of the devised films, they were soaked in the prepared various molar KOH solutions for different intervals of time. It is well established that uptake of solution in a polymer depends majorly on the pH of the solution it is soaked in <sup>22-25</sup>. Thus, prior to any swelling experiments, pH values of each of the KOH (2-8M) solutions were measured using a digital pH meter. The pH values recorded of the varied solutions ranged from 12.84 – 13.98 based on molar concentration (figure S2(a)). Using the measured weights pre- and post-soaking, the swelling ratio (SR) for each of the {X}CP samples was calculated using the relation:  $SR = (W2-W1)/W1$  and plotted for each of the time intervals (figure S2(b)).

Results analysis indicated that all samples in varied molarity KOH solutions observed the highest SR within 45 min. of soaking, following which they remained constant with increasing

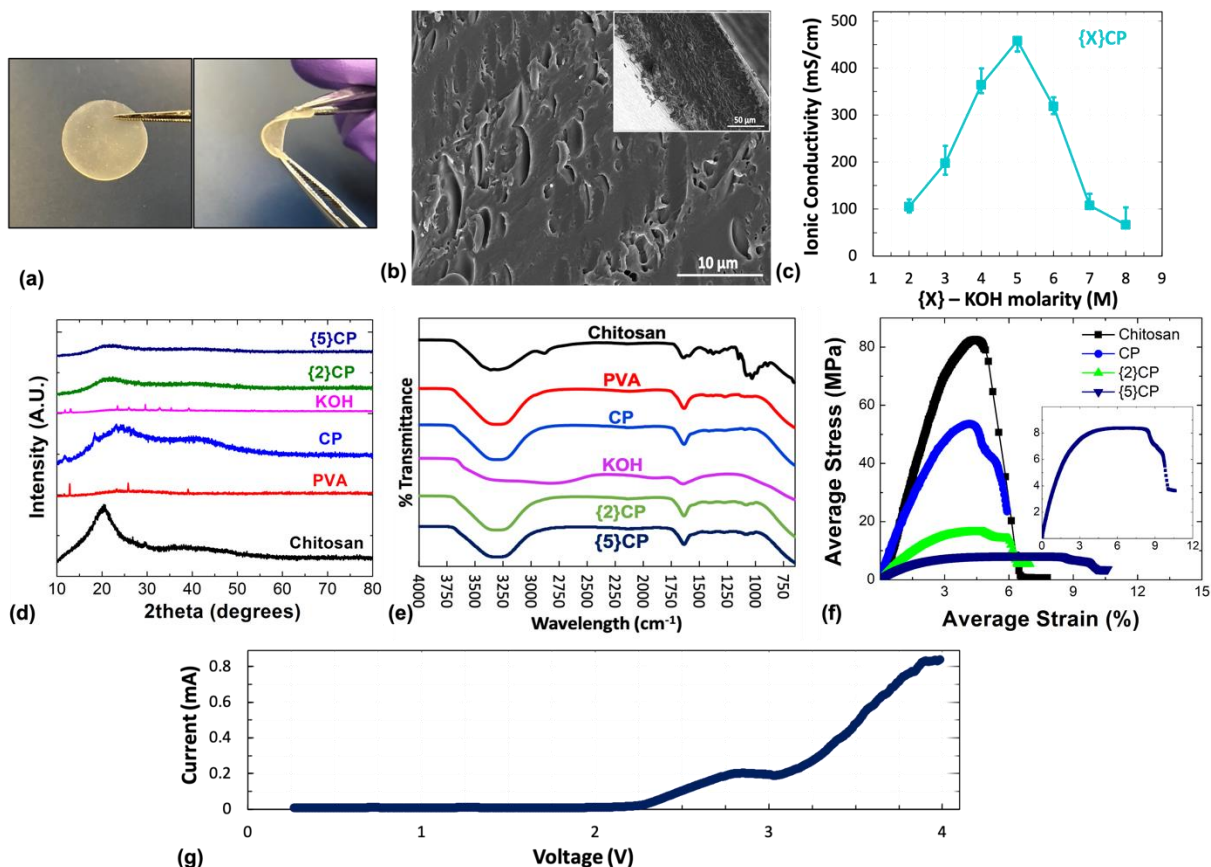


Figure 2. (a) Images of free standing and bent CP sample; (b) SEM of {5} CP sample (inset – cross section); (c) Ionic conductivities trend with different molar concentrations of KOH solutions used for making {X}CP samples; (d) XRD, (e) FTIR, and (f) Tensile stress-strain curves of Chitosan, CP, {2}CP and {5}CP samples; (g) Linear scan voltammogram for {5}CP sample sweep at 5mV/s.

soak time. It was also observed that SR values of the samples increased with increasing pH value until 13.49 (base scale); i.e. pH of 5M KOH solution. A highest SR of 2.1 was recorded for {5}CP sample. The SEM image of the aforementioned sample (figure 2(b)) indicated presence of number of pores on the surface and cross-sectionally. We assume this sponge-like structure helped retain higher amounts of KOH, as previously reported<sup>24</sup>. Swelling samples in KOH solutions with pH

values beyond 13.5 recorded comparatively lower SR. During experimentation, rapid visible salt crystal formations was observed for samples in 6, 7, and 8M KOH solutions with progress of time. The optical micrographs of samples soaked in 5, 6, and 7M KOH solutions for 45 min. (figure S3), confirm the enhanced salt crystal formations in {6}, {7}CP samples when compared to {5}CP sample. These excess salt formations may have resulted in the sample not being able to retain much of KOH due to lack of availability of volatile KOH; thereby resulting in lower SR<sup>22,23</sup>. All samples ({X}CP) were further tested for ionic conductivities to assess their performances and also to understand the effect of swelling on the performance.

The ionic conductivities of each of the {X}CP samples were calculated and can be seen in figure 2(c). The plot shows an increase in ionic conductivity with increased KOH concentrations until 5M and reduction beyond. A highest ionic conductivity of 457.19 mS/cm was recorded for {5}CP sample. The increase in conductivity until 5M might be due to increase in the number of mobile OH<sup>-</sup> ions resulting from better amorphicity, and reduction beyond 5M due to aggregation of excess ions<sup>24,36</sup>. This trend of increasing values until 5M KOH and then reducing beyond is also similar to the trend of SR ratios obtained for varied samples. Hence, we assume these increase in ionic conductivities until 5M is resultant of higher swelling ratios and is in agreement with previously reported studies. To further validate the achievement of better amorphicities through PVA and KOH addition to chitosan, XRD analysis was performed.

The XRD spectra obtained (figure 2(d)) indicated that with addition of PVA to chitosan, the (0 2 0) and (1 1 0) characteristic peaks broadness increased and intensity decreased. This indicated

the increase in amorphous nature of the gel matrix with addition of PVA, and is in agreement with previously reported <sup>17,24</sup>. With further addition of KOH (2M and 5M), a heightened amorphous domain was evident from relaxation of all peaks. This confirmed the presence of more OH<sup>-</sup> ions within the CP electrolyte when swelled in KOH. Furthermore, evaluation of the deconvoluted peaks (figure S4) obtained from each of the samples respective spectra for crystallinity index indicated reduction in crystallinity by 25% with PVA addition to chitosan; and a reduction by 6.6% & 27.4% when CP samples were swelled in 2M and 5M respectively, validating the improvement in amorphicity observed. Additionally, the crystallinity index values obtained (table S1) also further validated that the {5}CP sample was more amorphous than {2}CP sample. This explains the better ionic conductivity of {5}CP observed in comparison to {2}CP. FTIR analysis of the desired samples was also performed to confirm structural changes within the samples with additives. Figure 2(e) shows the spectra obtained. Table S2 provides IR bands and their corresponding bonds observed for pure chitosan, PVA and KOH. The spectra obtained were similar to previously reported <sup>24-26</sup>. Spectra for CP indicated relaxing of most stretches when compared to pure chitosan, thus confirming definite changes in bonds. Further, incorporation of KOH (2M/5M) in CP indicated re-emergence of tiny characteristic peaks between 1023 – 1158 cm<sup>-1</sup>, along with small disturbances signifying bond changes and vibrations <sup>24</sup>.

The thermal and mechanical properties of the best performing {5}CP electrolyte sample were also studied and compared to our previously reported chitosan, CP and {2}CP data <sup>24</sup>, to thoroughly understand its potential for use in batteries. The thermogram obtained for {5}CP had similar characteristics as {2}CP and is safe for use under 50° (figure S5, table S3). Figure 2(f) and

table S4 show the tensile stress-strain curve and mechanical properties exhibited by {5}CP sample respectively in comparison to others. It was observed that with the incorporation of both PVA and KOH (2M/5M) additives, chitosan's excellent stress properties were reduced. This trend in reduction of strength with additives was similar to various polymer electrolytes reported with additives<sup>39,40</sup>. However, the ductile nature of the sample with 5M KOH was drastically improved. This might be due to the incorporation of higher amounts of KOH within the system, allowing a higher stretch of bonds. Though a decrease in stress properties was observed for {5}CP, it is still a suitable candidate for use in flexible batteries as stresses above 5 MPa are rarely observed in most flexible battery applications. Additionally, the strain rate observed (~10%) allows it to be suitable for use in moderate stretchable applications too. The best sample {5}CP was furthermore tested for electrochemical stability in the Zinc electrodes system. The voltammogram obtained from LSV (figure 2(g)) showed negligible current densities within 0-2 V range and beyond that an increase in currents was observed. Hence it was deduced that the prepared {5}CP electrolyte sample possesses the necessary electrochemical stability in a zinc-based system when operated under 2 V potentials. Overall, the prepared biodegradable chitosan-based alkaline polymer electrolyte with excellent ionic conductivity, flexibility and stability is among the best reported (table S5).

### **Cell fabrication and testing**

Zn-EMD cells were prepared using the devised electrolyte and cathode (as illustrated in figure1(a)) for testing. Additionally, a large cell was also fabricated and bent manually several

times (figures 1(b) - (d)) to demonstrate flexibility of overall cell. Cell testing was performed at room temperature using a two-electrode setup in which, EMD was chosen as the working electrode and zinc foil was chosen as the counter and reference electrode. In this study, we explore the performance of the constructed batteries at different potential limits. The limits used for electrochemical testing were 0.4 – 1.2 V and 0.4 – 1.6 V vs Zn ( $\text{Zn}^{2+}/\text{Zn}$ ). The lower limit of 0.4 V was chosen due to the fact that EMD undergoes a two-step reduction process from its complexation reactions; resulting in higher capacity utilizations<sup>27-30,32,34,37</sup>. For the upper bound, 1.6 V was chosen for testing because the oxidation reactions necessary for Mn to convert back to its +4 state after its discharge process occur under this potential<sup>27,34</sup>. Gradual changes in the structure of EMD to highly irreversible  $\delta\text{-MnO}_2$  occurs during the oxidation process between 1.3 - 1.5 V potential<sup>27,32,34</sup>. Thus, another potential 1.2 V was chosen as a higher limit for one of the testing conditions anticipating reduction in polymorphic changes of EMD.

Figure 3(a) shows the cyclic voltammograms of the assembled Zn-EMD cells swept at 5 mV/s within 0.4 -1.2 V (Low) and 0.4 – 1.6 V (High) potential ranges respectively. The electrochemical scan for the high voltage range clearly shows a large wide reduction peak corresponding to proton insertion, i.e. integration of protons into the EMD ( $\gamma\text{-MnO}_2$ ) lattice, leading to formation of  $\alpha\text{-MnOOH}$  phase in the 1 – 1.4 V region<sup>27-32</sup>. Also, two distinguishable oxidation peaks at approximately 0.9 V and 1.3 V were observed in the anodic direction signifying oxidation of  $\text{Mn}^{3+}$  to  $\text{Mn}^{4+}$  state<sup>27,34</sup>. Similarly, for the low voltage range scan, a large reduction peak at 0.9 V and a small oxidation peak at 0.8 V were observed signifying the changes occurring in the oxidation

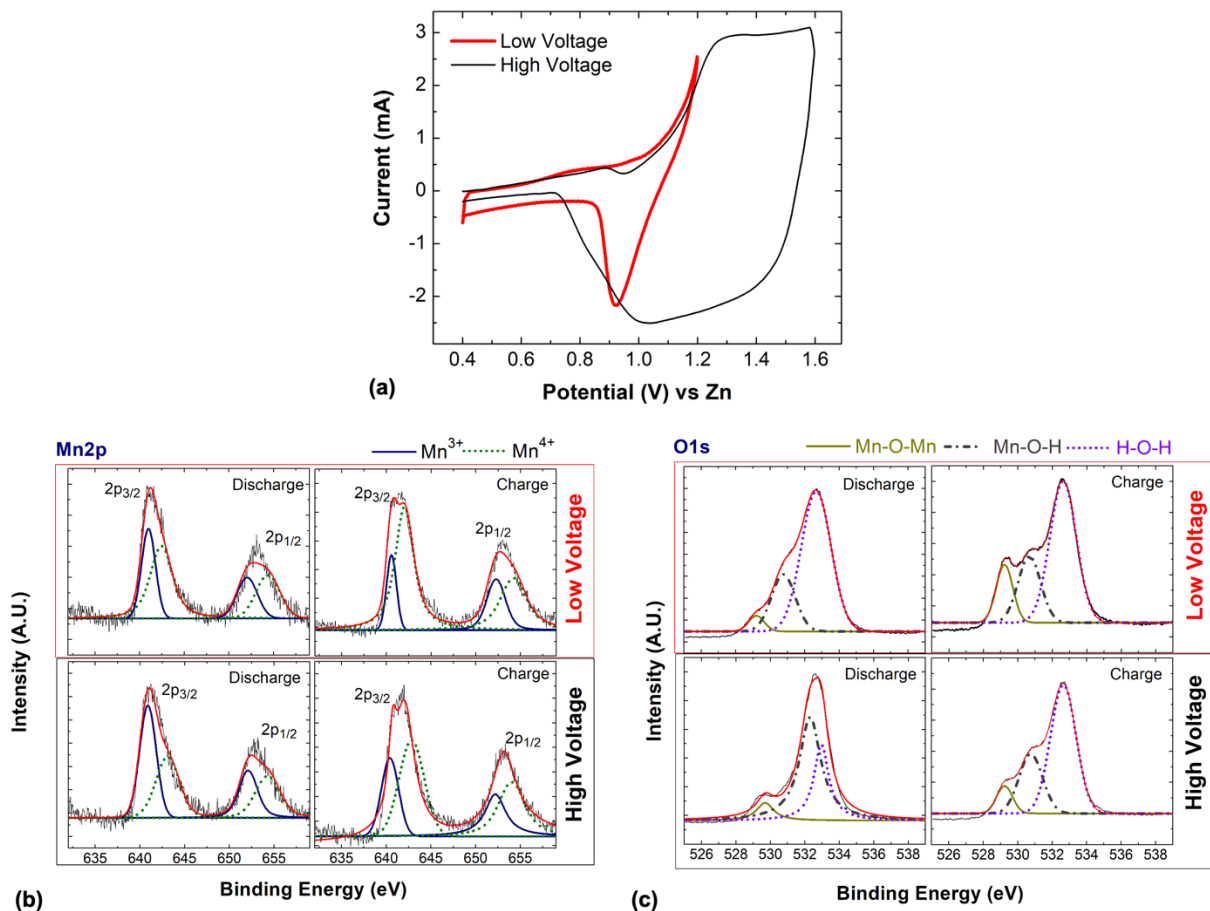


Figure 3. (a) Voltammograms of the constructed cells swept at 5mV/s for high (0.4 – 1.6 V) and low (0.4 – 1.2 V) voltage ranges; (b) Mn 2p, and (c) O 1s XPS spectra for the cathode at first charged and discharged states for low and high ranges.

states of Mn. The potential difference ( $\Delta E_p$ ) between the major anodic and cathodic peaks were found to be 250 and 120mV for high and low voltage windows respectively, suggesting that achieving reversibility is much easier in the low voltage condition <sup>38</sup>. Moreover, the cyclic voltammetry results indicate that in both cases, only a single-electron transfer was entailed. The

changes in oxidation states of Mn for the two potential ranges, i.e., high and low, were confirmed by performing XPS on the cathodes in charged and discharged states respectively.

As can be seen in figure 3(b), the Mn 2p region mainly consists the spin-orbit doublet peaks of Mn2p<sub>1/2</sub> and Mn2p<sub>3/2</sub> states at approximately 653 and 641.5 eV respectively, for charged and discharged states for both low and high voltage ranges. The deconvoluted Mn 2p spectra (Mn<sup>3+</sup> and Mn<sup>4+</sup> signals) indicate changes in signal intensities between the discharged and charged states for both ranges, confirming changes in valence states of Mn. To name one, when comparing Mn<sup>3+</sup> and Mn<sup>4+</sup> signals of 2p<sub>3/2</sub> orbit in low range (top images in figure 3(b)), reduction in intensity of Mn<sup>3+</sup> signal can be clearly observed. Whereas, intensity of Mn<sup>4+</sup> increased when the cell was charged to 1.2V from its 0.4V discharged state. This intensity shift confirms the successful conversion of Mn from Mn<sup>3+</sup> to Mn<sup>4+</sup> when being charged. Additionally, the O 1s spectra was fitted with three components, i.e. H-O-H bond at ~532.5 eV for materials water residue, Mn-O-H bond at ~530.6 eV for the absorbed MnOOH, and Mn-O-Mn bond at ~529.2 eV for MnO<sub>2</sub>. Successful formations of MnOOH and MnO<sub>2</sub> in discharged and charged states were observed for both ranges when analysed. Furthermore, it was also observed that a significantly stronger Mn-O-H bond was observed when the cell was discharged in high voltage range. This suggests formation of additional MnOOH at the region by intercalation into MnO<sub>2</sub><sup>39</sup> and is consistent with Mn<sup>3+</sup> formations observed from Mn 2p. These formations make seem high range superior for conversion to Mn<sup>3+</sup> in comparison to low voltage range. But, the weakened Mn-O-Mn bond indicates bond breakages in MnO<sub>2</sub> and possible internal structural changes and/or intercalation of Zn<sup>2+</sup> with MnO<sub>2</sub>

causing increased formations of irreversible  $\delta$ -MnO<sub>2</sub> or ZnMn<sub>x</sub>O<sub>y</sub> complexes as a result<sup>39</sup>. It agrees with reversibility analysis from low and high voltage range voltammetry results.

The assembled cell was further made to undergo typical galvanostatic cycling tests at charge and discharge current densities of 0.1 A/g for different potential windows. A protocol of constant-current discharge until 0.4V followed by rest for 120 seconds before the constant-current charge up to 1.2 V or 1.6 V was followed for the galvanostatic charge-discharge (GCD) test. Figures 4(a) & (b) show the charge-discharge profiles for the initial 5 cycles of the assembled cell cycled within the low and high voltage ranges respectively at 0.1 A/g. Highest specific capacities of 310mAh/g and 287mAh/g were recorded for the initial cycles of cells tested between low and high voltage ranges respectively. It was observed that with further cycling, reduction in capacities were observed for both. We assume this capacity fade in initial cycles may be due to fast Mn ions dissolution from the EMD cathode, resulting from active material losses due to interactions with strong alkaline solution<sup>28,30,37,40</sup>. This phenomenon of capacity losses during initial cycles are a typical characteristic of Zn-MnO<sub>2</sub> alkaline batteries<sup>30,37</sup>. Though the initial specific capacity value seemed to be similar for both ranges, over cycling it was observed that the rate of capacity fade in the high voltage range tested cell was much more predominant than that of the low range tested cell. These specific capacities averaged to ~230mAh/g and 50mAh/g respectively for low and high voltage ranges over 50 cycles, resulting in 74% and 17.4% capacity retentions with respect to initial cycles (figure 4(c)). We hypothesize that the higher reductions in capacities for the high voltage range was due to increased inactive  $\delta$ -MnO<sub>2</sub> or Zn-MnO<sub>2</sub> complex formations. They are

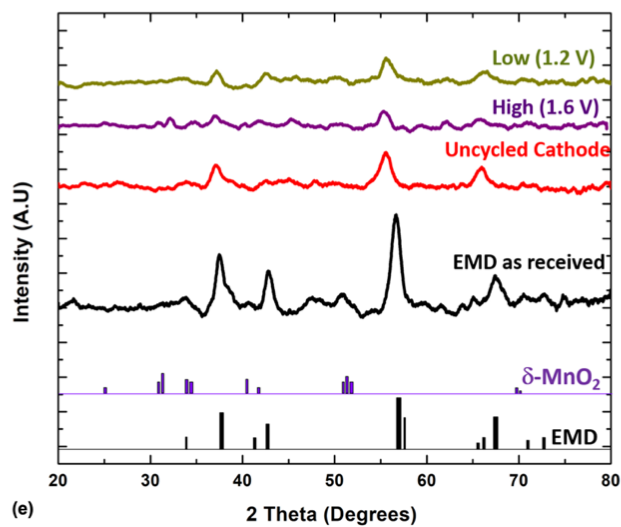
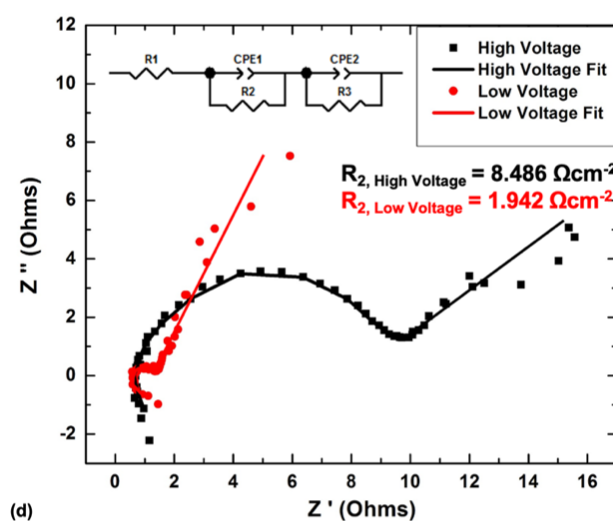
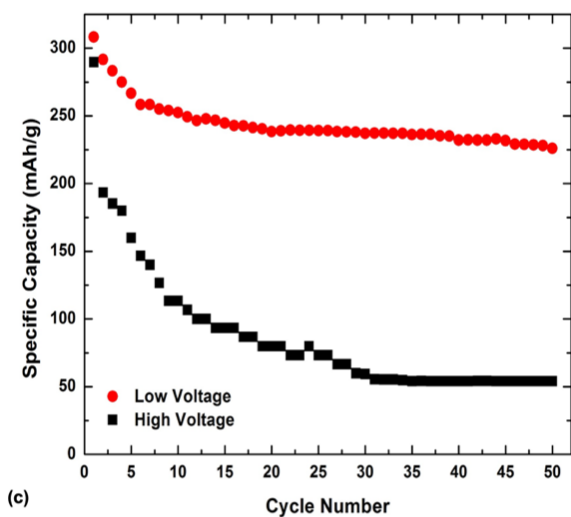
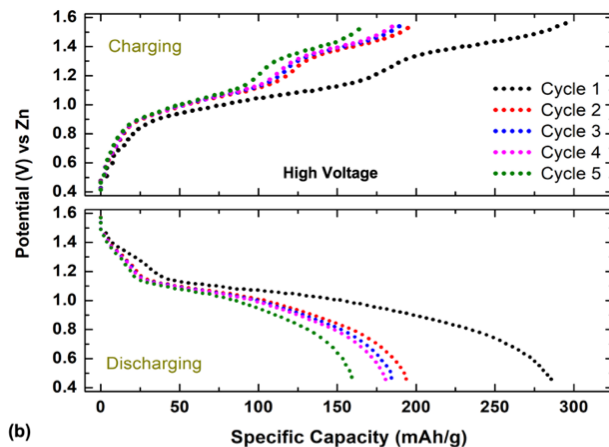
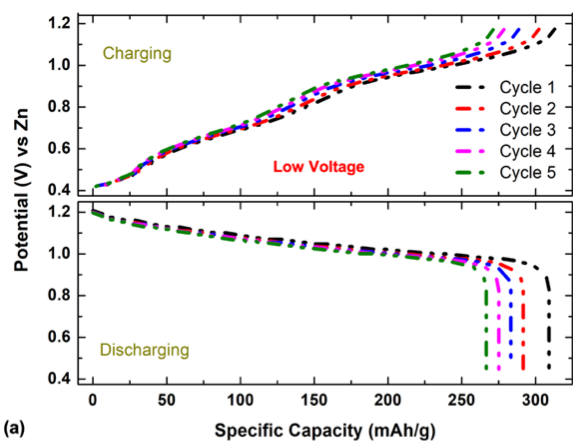


Figure 4. Varied charge-discharge profiles for the Zn-EMD cell cycled in the (a) low; and (b) high voltage ranges respectively; (c) Galvanostatic cycle life data for the assembled cells cycled at 0.1A/g; (d) Impedance plot of cells post 50 cycles in high and low voltage ranges; (e) XRD spectra of EMD powders as received, prepared cathode prior to any cycling, and cathodes from cells after 50 cycles stopped on charge for both potential ranges respectively.

highly irreversible and unfit for further use due to their disturbed tunnel structure, unless Cu, Bi, Ti, or their oxides are used as additives to EMD during cathode preparation <sup>27,30,32,34</sup>.

It has been previously reported that inactive compound formations from repeated cycling generally increases resistance for charge transfer between the electrolyte and electrode layers and resultantly contribute to capacity decay <sup>27</sup>. Impedance analysis was conducted on the cells cycled at 0.1A/g for 50 times at both high and low voltage ranges to investigate the same. The impedance spectra obtained along with the line fit and the equivalent circuit used are shown in figure 3(e). The charge transfer resistance ( $R_2$ ) recorded for the cell that underwent 50 cycles in the high voltage range, was ~4.3 times higher than that of a cell with same conditions cycled in the low voltage range. Therefore, it can be deduced that inactive phase formations are much more predominant in the high voltage range and contribute to higher capacity decay as a result than in low range. Ex-situ XRD analysis was also performed on the cathodes of cells cycled 50 times respectively in the high and low potential regions and stopped on charge. The spectra obtained (figure 4(f)) confirms the conversion of EMD to  $\delta$ -MnO<sub>2</sub> in both the potential ranges. However, the obtained peaks intensity indicates lower  $\delta$ -MnO<sub>2</sub> formations in the low voltage region in comparison to higher voltage regions. Thus, XRD validates our earlier hypothesis of reduced capacities due to presence of higher inactive phases. ZnMn<sub>x</sub>O<sub>y</sub> complex formations weren't detectable in the XRD spectra. We assume

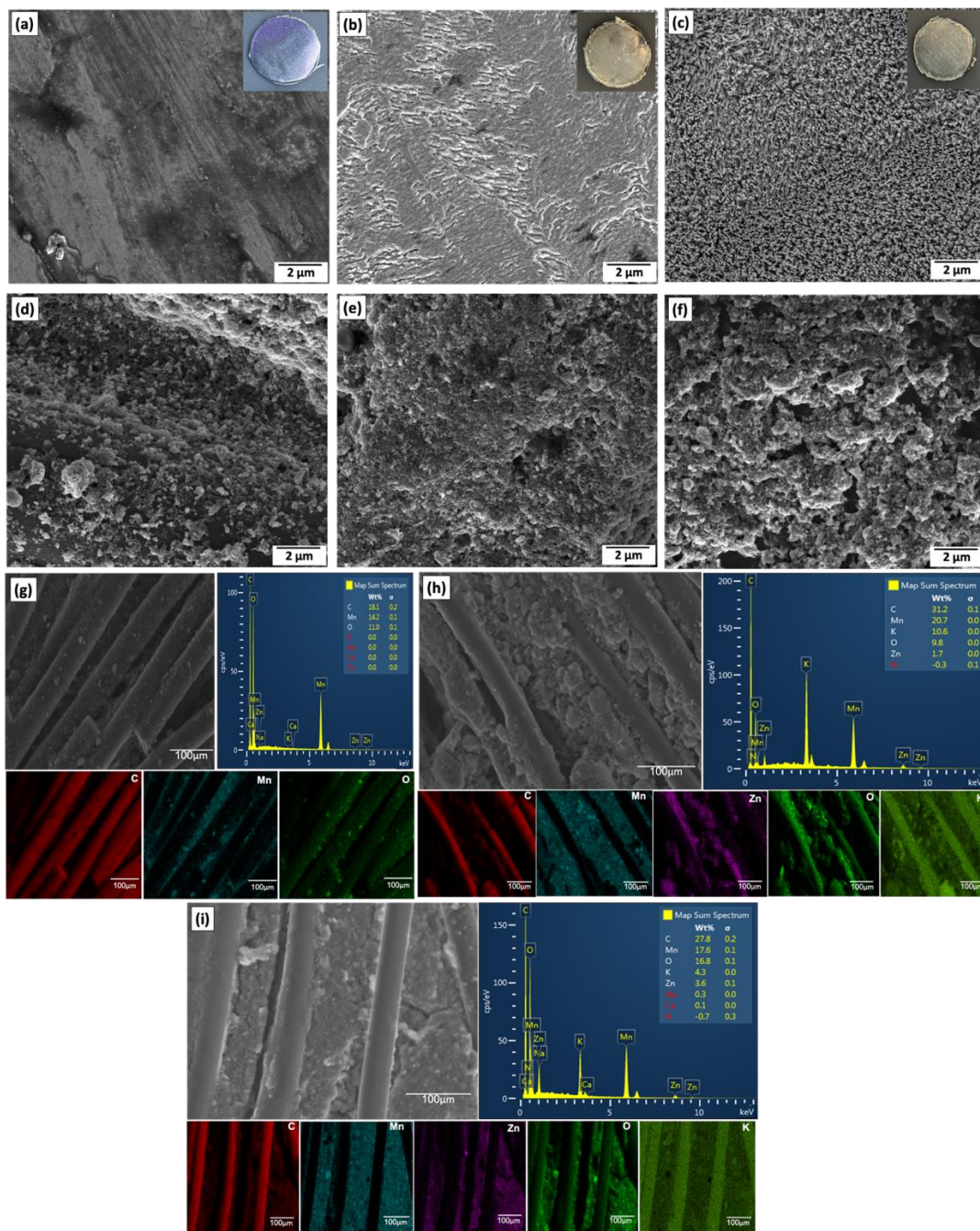


Figure 5. Scanning electron microscopic images of electrodes (Zn anode and EMD cathode) before and after 100 cycles, stopped at charge for both potential ranges. (a)-(c) Zinc anode; (d)-(f) EMD Cathode and their corresponding EDX spectra (g)-(i).

this might be due to the presence of lower amounts in comparison.

Further characterizations of the anode and cathode before and after 100 cycles are shown in figure 5. Figure 5(a) – (c) indicate the SEM images of Zinc anode before and after 100 cycles for low and high range respectively. The images clearly show shape changes happening on the surfaces of all cycled anodes. However, pronounced shape changes (longer lengths) were observed on the anode of the cell cycled in the high voltage range comparatively, signifying quicker dendrite growth and premature failure as a result if dendrite propagation occurs <sup>5,6</sup>. 5(d) – (i) indicate the SEM micrographs and relative EDX spectra for the EMD cathodes before and after 100 cycles in both potential ranges. No prominent electrode degradation was observed on the cathode side when comparing before and after cycling (any voltage) images. The EDX spectra for the cathodes show that Zinc was present on both low and high voltage cycled cathode, confirming  $\text{ZnMn}_x\text{O}_y$  complex formations during cycling over several cycles, which otherwise wasn't present prior to cycling. When comparing the presence of zinc in terms of wt.%, it was observed that the cathode cycled in the high voltage region had twice as much of zinc in the low voltage region. These irreversible complex formations also result in capacity fade and thus validating higher capacity losses in high-voltage regions.

To examine the performance and extent of reversibility achievable for a Zn-EMD alkaline battery without any electrode additives, further electrochemical tests were conducted in the low voltage (0.4-1.2V) region. The Zn-EMD cell demonstrates good rate performance as shown in figures 6(a) & (b). The average discharge capacities were 287.6, 217.2, 200.24, 188.4, and 132.6

mAh/g respectively at 0.1, 0.2, 0.3, 0.5, and 1 A/g current densities. Moreover, when the rate was switched back to 0.1 and 0.5 A/g, discharge capacities of 225 and 178 mAh/g respectively were recovered, revealing reasonably good structural stability and a considerable tolerance to rapid  $\text{Zn}^{2+}$  complexations<sup>5</sup>. Figure 6(c) shows the cycling capability of the cell obtained from low voltage range GCD test conducted at 0.5 A/g current density over 300 cycles. A highest average specific capacity of 248.5 mAh/g was recorded, after which rapid loss in capacity values were observed as earlier. The rate of loss in capacity values after 60 cycles was comparably low and stabilizes to an average capacity of 175 mAh/g over 300 cycles. Figure 6(c) also shows the 96.5% coulombic efficiency obtained. Figure S6 indicates the capacity retention values calculated using initial capacity. A drastic fall was observed within the first 15 cycles, beyond which gradual changes were recorded. Additionally, discharge curves for cycles 1 and 100 at 0.5 A/g were also shown in figure 6(d). The discharge plateaus can easily be discerned from the curves and are also in accordance with the reduction peak of the CV curve. When analysing the curves, it was observed that most of the capacity obtained was over 0.9 V potential. Energy densities of 150.4 – 252.4 Wh/kg (calculated w.r.t mass of the cathode) are achievable for these systems.

Furthermore, the assembled cell was also tested for performance under different bending conditions by mounting and securing the assembled flexible large cell in such a way that it is bent at a particular radius under galvanostatic charge-discharge testing conducted at 1 A/g current density. As can be seen from figure 6(e), the discharge curves obtained for different bending radii almost overlap with the initial flat state, thus indicating robust performance of the cell even under deformation without much capacity deteriorations. This indicates good performance stability of

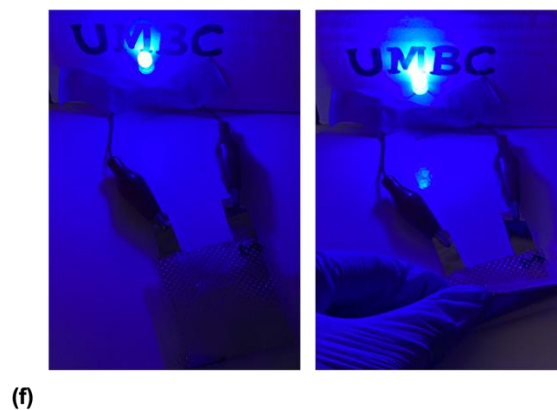
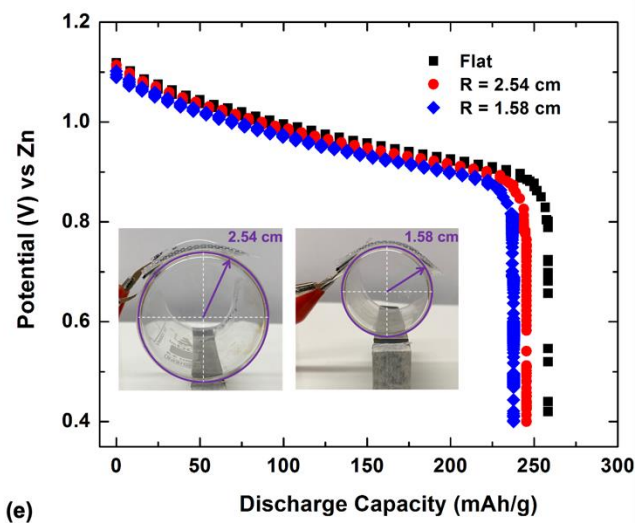
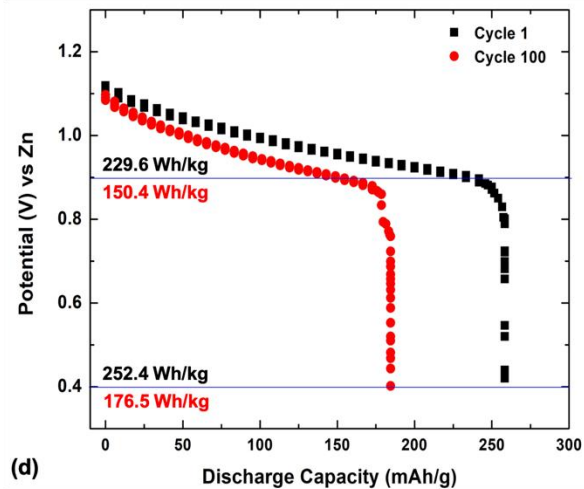
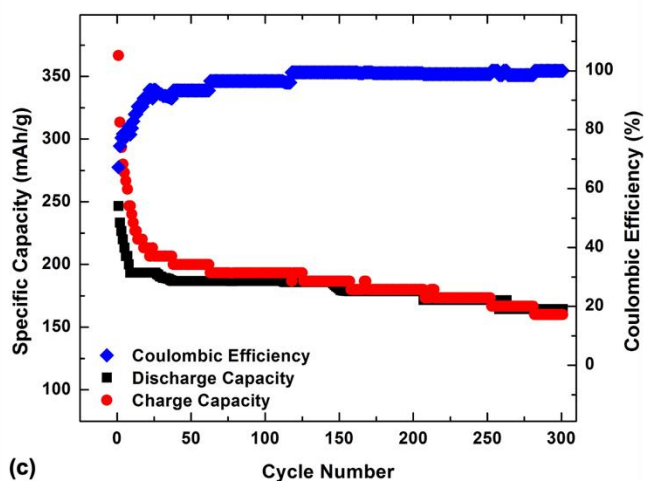
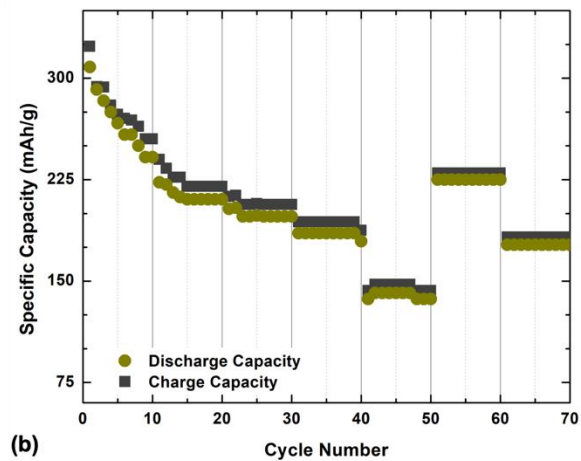
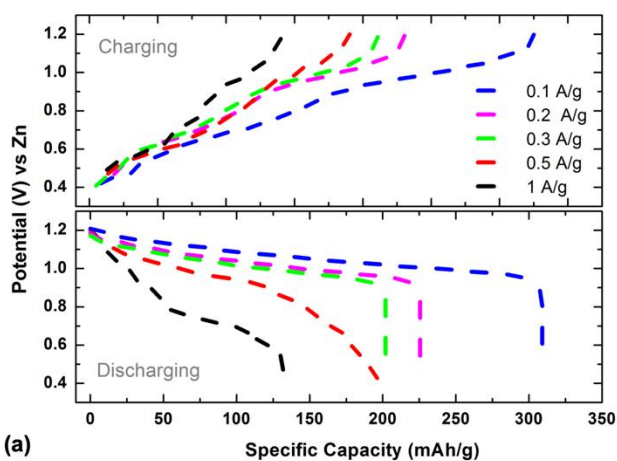


Figure 6. (a) Charge-discharge profiles of the assembled cells run at different current densities; (b) Rate Capability of the Zn-EMD cell with the novel Chitosan-alkaline electrolyte cycled between 0.4 – 1.2V; (c) Cycling performance at 0.5 A/g; (d) Discharge curves for cycle 1 and cycle 100 till 0.4V at 0.5 A/g with energy density (w.r.t. cathode mass) shown; (e) Initial bending performance of the assembled large cell in different bending conditions; and (f) Photographs of a LED bulb powered by a flexible Zn-EMD battery in the original and bend states.

the cell even when physically bent. Moreover, the battery constructed by using 3 cells in series, successfully powered a LED bulb when flat and bent as can be observed from figure 6(f). Thus, the assembled Zn-EMD with the devised novel highly ionically conducting chitosan-based alkaline polymer electrolyte demonstrates its promising potential in personalized wearable electronics. The high reversibility recorded for these prepared Zn-EMD alkaline chemistries with polymer electrolyte and no cathode additives is one of the first reported. The results obtained are also comparable to the Zn-EMD cells with aqueous alkaline mediums and cathode additives (table S6).

## Conclusions

A safe, novel, flexible, highly ionically conducting chitosan-based alkaline electrolyte was devised using an optimized technique. Also, a cell was constructed with various devised battery layers by using a non-conventional assembly technique designed to achieve good contact between the layers. Results from the electrochemical tests conducted on the fabricated Zn-EMD cells indicate successful incorporation of the polymer electrolyte into the system. Considerably good rate performance and reversibility of the constructed Zn-EMD cells was also achieved; due to reduced inactive phase formations as a result of limited (low) potential range (0.4 – 1.2 V)

electrochemical testing. Also, the demonstrated physical flexibility of the large cell constructed extends its potential use in flexible and wearable storage applications.

## **Conflicts of interest**

The authors declare no conflict of interest.

## **Acknowledgements**

The authors would like to acknowledge support from University of Maryland Baltimore County (UMBC) for supporting this research through start-up fund. The authors would also like to thank Dr. Mark Allen for unrestricted access to his lab and equipment, and also Eunhwa Jang, Preetham Gowni, Micah Thorpe and Renmar Sarreal for their contributions.

## **Supporting Information**

Optical micrographs of Chitosan, CP samples, {5}CP, {6}CP, and {7}CP samples; pH variation chart of various KOH solutions; Swelling ratios of soaked {X}CP samples in varied KOH solutions for different intervals of time; Peak-deconvolution curve fitting assuming gaussian functions for each peak of XRD spectra and their corresponding peaks and crystallinity index data for Chitosan, CP, {2}CP, and {5}CP samples; IR-spectra summary of pure Chitosan, PVA, and KOH; Thermograms and analysis summary of Chitosan, CP, {2}CP, and {5}CP samples; Mechanical properties of Chitosan, CP, {2}CP, and {5}CP samples; Comparison of ionic conductivities of various bio-degradable polymer electrolytes; Capacity retention curve of the Zn-

EMD cell with novel chitosan-alkaline electrolyte cycled between 0.4 – 1.2 V; Comparison of various Zn-MnO<sub>2</sub> alkaline chemistry systems performances.

## References

1. Dunn, B.; Kamath, H.; Tarascon, J. M., Electrical energy storage for the grid: a battery of choices. *Science* 2011, 334 (6058), 928-35.
2. Larcher, D.; Tarascon, J. M., Towards greener and more sustainable batteries for electrical energy storage. *Nat Chem* 2015, 7 (1), 19-29.
3. Wanger, T. C., The Lithium future-resources, recycling, and the environment. *Conservation Letters* 2011, 4 (3), 202-6.
4. Jacoby, M., Safer lithium-ion batteries. *Chem. Eng. News* 2013, 91 (6), 33-7.
5. Ming, J.; Guo, J.; Xia, C.; Wang, W.; Alshareef, H. N., Zinc-ion batteries: Materials, mechanisms, and applications. *Materials Science and Engineering: R: Reports* 2019, 135, 58-84.
6. Li, H.; Ma, L.; Han, C.; Wang, Z.; Liu, Z.; Tang, Z.; Zhi, C., Advanced rechargeable zinc-based batteries: Recent progress and future perspectives. *Nano Energy* 2019, 62, 550-87.
7. Li, Z.; Young, D.; Xiang, K.; Carter, W.; Chiang, Y. M., Towards high power high energy aqueous sodium-ion batteries: The NaTi<sub>2</sub>(PO<sub>4</sub>)<sub>3</sub>/Na<sub>0.44</sub>MnO<sub>2</sub> system. *Advanced Energy Materials* 2013, 3(3), 290-4.
8. Wessells, C. D.; Peddada, S. V.; Huggins, R. A.; Cui, Y., Nickel hexacyanoferrate nanoparticle electrodes for aqueous sodium and potassium ion batteries. *Nano Letters* 2011, 11 (12), 5421-5.
9. Kundu, D.; Adams, B. D.; Duffort, V.; Vajargah, S. H.; Nazar, L. F., A high-capacity and long-life aqueous rechargeable zinc battery using a metal oxide intercalation cathode. *Nature Energy* 2016, 1(10), 1-8.
10. Zhang, S. S., A review on the separators of liquid electrolyte Li-ion batteries. *Journal of Power Sources* 2007, 164 (1), 351-64.
11. Merle, G.; Hosseiny, S. S.; Wessling, M.; Nijmeijer, K., New cross-linked PVA based polymer electrolyte membranes for alkaline fuel cells. *Journal of Membrane Science* 2012, 409, 191-9.
12. Patel, S.K.; Awadhia, A.; Agrawal, S.L., Thermal and electrical studies on composite gel electrolyte system: PEG–PVA–(NH<sub>4</sub>CH<sub>2</sub>CO<sub>2</sub>)<sub>2</sub>. *Phase Transitions* 2009, 82(6), 421-32.

13. Kumar, G. G.; Sampath, S., Electrochemical characterization of poly(vinylidene fluoride)-zinc triflate gel polymer electrolyte and its application in solid-state zinc batteries. *Solid State Ionics* 2003, 160 (3-4), 289-300.
14. Wu, G. M.; Lin, S. J.; Yang, C. C., Alkaline Zn-air and Al-air cells based on novel solid PVA/PAA polymer electrolyte membranes. *Journal of Membrane Science* 2006, 280 (1-2), 802-8.
15. Mohamad, A. A.; Mohamed, N. S.; Yahya, M. Z. A.; Othman, R.; Ramesh, S.; Alias, Y.; Arof, A. K., Ionic conductivity studies of poly(vinyl alcohol) alkaline solid polymer electrolyte and its use in nickel–zinc cells. *Solid State Ionics* 2003, 156 (1-2), 171-7.
16. Santos, F.; Tafur, J. P.; Abad, J.; Fernández Romero, A. J., Structural modifications and ionic transport of PVA-KOH hydrogels applied in Zn/Air batteries. *Journal of Electroanalytical Chemistry* 2019, 850, 113380.
17. Poosapati, A.; Negrete, K.; Jang, N.; Hu, L.; Lan, Y.; Madan, D., Wood cellulose-based thin gel electrolyte with enhanced ionic conductivity. *MRS Communications* 2019, 9 (3), 1015-21.
18. Kumar, G.G.; Sampath, S., Electrochemical characterization of a zinc-based gel-polymer electrolyte and its application in rechargeable batteries. *Journal of The Electrochemical Society* 2003, 150(5), A608.
19. Poosapati, A.; Jang, E.; Madan, D.; Jang, N.; Hu, L.; Lan, Y., Cellulose hydrogel as a flexible gel electrolyte layer. *MRS Communications* 2019, 9 (1), 122-8.
20. Li, H.; Han, C.; Huang, Y.; Zhu, M.; Pei, Z.; Xue, Q.; Wang, Z.; Liu, Z.; Tang, Z.; Wang, Y.; Kang, F.; Li, B.; Zhi, C., An extremely safe and wearable solid-state zinc ion battery based on a hierarchical structured polymer electrolyte. *Energy & Environmental Science* 2018, 11(4), 941-51.
21. Park, J.; Park, M.; Nam, G.; Lee, J.S.; Cho, J., All-solid-state cable-type flexible zinc–air battery. *Advanced Materials* 2015, 27(8), 1396-401.
22. Feldman, D.; Barbalata, A., *Synthetic Polymers: technology, properties, applications*. Springer Science & Business Media 1996.
23. Molyneux, P., *Water-soluble synthetic polymers: volume II: properties and behavior*. CRC press 2018.
24. Poosapati, A.; Negrete, K.; Thorpe, M.; Hutchison, J.; Zupan, M.; Lan, Y.; Madan, D., Safe and flexible chitosan-based polymer gel as an electrolyte for use in Zinc-alkaline based chemistries. *Journal of Applied Polymer Science* 2021, accepted.
25. Rinaudo, M., Chitin and chitosan: properties and applications. *Progress in Polymer Science* 2006, 31 (7), 603-32.

26. Bhad, S.N.; Sangawar, V.S., Synthesis and study of PVA based gel electrolyte. *Chemical Science Transactions* 2012, 1(3), 653-7.
27. Yadav, G. G.; Gallaway, J. W.; Turney, D. E.; Nyce, M.; Huang, J.; Wei, X.; Banerjee, S., Regenerable Cu-intercalated MnO<sub>2</sub> layered cathode for highly cyclable energy dense batteries. *Nature Communications* 2017, 8 (1), 1-9.
28. Huang, J.; Yadav, G. G.; Gallaway, J. W.; Wei, X.; Nyce, M.; Banerjee, S., A calcium hydroxide interlayer as a selective separator for rechargeable alkaline Zn/MnO<sub>2</sub> batteries. *Electrochemistry Communications* 2017, 81, 136-40.
29. Yadav, G.G.; Cho, J.; Turney, D.; Hawkins, B.; Wei, X.; Huang, J.; Banerjee, S.; Nyce, M., Going beyond intercalation capacity of aqueous batteries by exploiting conversion reactions of Mn and Zn electrodes for energy-dense applications. *Advanced Energy Materials* 2019, 9(48), 1902270.
30. Biswal, D. A.; Tripathy, B.C.; Sanjay, K.; Subbaiah, T.; Minakshi, M., Electrolytic manganese dioxide (EMD): a perspective on worldwide production, reserves and its role in electrochemistry. *RSC Advances* 2015, 5(72), 58255-83.
31. Nesvaderani, F.; Bonakdarpour, A.; Wilkinson, D., pH-Controlled Electrolysis of Electrolytic Manganese Dioxide (EMD) for Improved Cycle Life of Rechargeable MnO<sub>2</sub>/Zn Batteries. *Journal of The Electrochemical Society* 2017, 164(4), A810-A819.
32. Yadav, G. G.; Wei, X.; Huang, J.; Gallaway, J. W.; Turney, D. E.; Nyce, M.; Secor, J.; Banerjee, S., A conversion-based highly energy dense Cu<sup>2+</sup> intercalated Bi-birnessite/Zn alkaline battery. *Journal of Materials Chemistry A* 2017, 5 (30), 15845-54.
33. Mehta, S.A.; Bonakdarpour, A.; Wilkinson, D.P., Impact of cathode additives on the cycling performance of rechargeable alkaline manganese dioxide–zinc batteries for energy storage applications. *Journal of Applied Electrochemistry* 2017, 47(2), 167-81.
34. Yadav, G. G.; Wei, X.; Huang, J.; Turney, D.; Nyce, M.; Banerjee, S., Accessing the second electron capacity of MnO<sub>2</sub> by exploring complexation and intercalation reactions in energy dense alkaline batteries. *International Journal of Hydrogen Energy* 2018, 43 (17), 8480-7.
35. Wang, Z.; Winslow, R.; Madan, D.; Wright, P. K.; Evans, J. W.; Keif, M.; Rong, X., Development of MnO<sub>2</sub> cathode inks for flexographically printed rechargeable zinc-based battery. *Journal of Power Sources* 2014, 268, 246-54.
36. Fan, L.; Wang, M.; Zhang, Z.; Qin, G.; Hu, X.; Chen, Q., Preparation and characterization of PVA alkaline solid polymer electrolyte with addition of bamboo charcoal. *Materials* 2018, 11(5), 679.

37. Qiu, F.; Huang, Y.; Hu, X.; Li, B.; Zhang, X.; Luo, C.; Li, X.; Wang, M.; Wu, Y.; Cao, H., An ecofriendly gel polymer electrolyte based on natural lignocellulose with ultrahigh electrolyte uptake and excellent ionic conductivity for alkaline supercapacitors. *ACS Applied Energy Materials* 2019, 2(8), 6031-42.
38. Ji, Y.; Liang, N.; Xu, J.; Zuo, D.; Chen, D.; Zhang, H., Cellulose and poly (vinyl alcohol) composite gels as separators for quasi-solid-state electric double layer capacitors. *Cellulose* 2019, 26(2), 1055-65.
39. Han, J.; Huang, Y.; Chen, Y.; Song, A.; Deng, X.; Liu, B.; Li, X.; Wang, M., High performances of gel polymer electrolyte based on chitosan-lignocellulose for lithium ion batteries. *ChemElectroChem* 2020, 7(5), 1213-24.
40. Wang, M.; Fan, L.; Qin, G.; Hu, X.; Wang, Y.; Wang, C.; Yang, J.; Chen, Q., Flexible and low temperature resistant semi-IPN network gel polymer electrolyte membrane and its application in supercapacitor. *Journal of Membrane Science* 2020, 597, 117740.
41. Pan, H.; Ellis, J. F.; Li, X.; Nie, Z.; Chang, H. J.; Reed, D., Electrolyte Effect on the Electrochemical Performance of Mild Aqueous Zinc-Electrolytic Manganese Dioxide Batteries. *ACS Applied Materials & Interfaces* 2019, 11 (41), 37524-30.
42. Minakshi, M.; Singh, P.; Carter, M.; Prince, K., The Zn–MnO<sub>2</sub> battery: The influence of aqueous LiOH and KOH electrolytes on the intercalation mechanism. *Electrochemical and Solid State Letters* 2008, 11(8), A145.
43. Han, M.; Huang, J.; Liang, S.; Shan, L.; Xie, X.; Yi, Z.; Wang, Y.; Guo, S.; Zhou, J., Oxygen Defects in  $\beta$ -MnO<sub>2</sub> Enabling High-Performance Rechargeable Aqueous Zinc/Manganese Dioxide Battery. *iScience* 2020, 23 (1), 100797.
44. Minakshi, M.; Biswal, D. A.; Tripathy, B.C., Electrodeposition of sea-urchin and cauliflower-like Ni/Co doped manganese dioxide hierarchical nanostructures with improved energy storage behavior. *ChemElectroChem* 2016, 3(6), 976-85.

Table of Contents (TOC) graphic

